INL/CON-09-15226
PREPRINT

Fast Reactor Subassembly Design Modifications for Increasing Electricity Generation Efficiency

Global 2009

R. Wigeland
K. D. Hamman

September 2009

The INL is a
U.S. Department of Energy
National Laboratory
operated by
Battelle Energy Alliance

Proceedings of Global 2009
Paris, France, September 6-11, 2009
Paper 9395

Fast Reactor Subassembly Design Modifications for Increasing Electricity Generation Efficiency

R. Wigeland and K. D. Hamman
Idaho National Laboratory
P.O. Box 1625
Idaho Falls, Idaho, U.S.A. 83415-3860
Tel: (208) 526-9840, Fax: (208) 526-2930,
Email: Roald.Wigeland@inl.gov

Abstract – *Fast reactors are being considered as one element of future nuclear power systems to enable continued use and growth of nuclear power by limiting high-level waste generation. However, their higher cost relative to existing nuclear reactor designs, even with their higher thermal efficiency, results in higher electricity costs making them economically less attractive to nuclear utilities. In an effort to increase thermal efficiency, fuel subassembly design changes are being investigated using computational fluid dynamics simulations. The goal of this study is to evaluate the effects that subassembly hexcan design changes can have on subassembly coolant flow, temperature distribution and hot channel factors. Simulations have been performed for a 19-pin subassembly geometry using typical fuel pin diameters and wire wrap spacers. The results have shown that it should be possible to raise the average coolant outlet temperature without increasing peak temperatures within the subassembly, allowing for higher thermal efficiency.*

I. INTRODUCTION

Given the ability of fast reactors to effectively transmute the transuranic elements that are present in spent nuclear fuel, fast reactors are being considered as one element of future nuclear energy systems to enable continued use and growth of nuclear power by limiting high-level waste generation. However, a key disadvantage of fast reactors is higher electricity cost relative to other nuclear reactor designs (due to higher initial cost), even though sodium-cooled fast reactors can operate with higher thermal efficiency. The economics of fast reactors are affected by the amount of electric power that can be produced from a reactor, i.e., the thermal efficiency for electricity generation.[1, 2] The present study examined the potential for fast reactor subassembly design changes to operate with higher thermal efficiency by raising the average coolant outlet temperature without increasing peak temperatures within the subassembly, i.e., to make better use of current technology.

Sodium-cooled fast reactors operate at temperatures far below the coolant boiling point, so that the maximum coolant outlet temperature is limited by the acceptable peak temperatures of the reactor fuel and cladding. Historically, fast reactor fuel subassemblies have been constructed using a large number of small diameter fuel pins contained within a tube of hexagonal cross-section, or hexcan. Past and present fast reactor designs and concepts utilize spacer grids or helical wound wire wraps to maintain spatial separation between fuel pins.[3, 4, 5, 6] In addition to providing a means for fuel pin spatial separation, wire wraps promote radial coolant mixing within a subassembly.

From a heat transfer and fluid flow perspective, it has been recognized for many years that the standard hexcan design was detrimental to achieving greater thermal efficiency, since it causes the fuel pins in the center of the subassembly to operate at higher temperatures than those near the hexcan walls.[7] Specifically, the standard hexagonal cross-section assembly design results in a larger coolant flow area next to the hexcan wall as compared to flow area in the interior of the subassembly. This results in a higher flow rate near the hexcan wall, overcooling the fuel pins adjacent to the wall, and a non-uniform coolant temperature distribution. It is the higher fuel and cladding temperatures for the interior fuel pins that limits the average coolant outlet temperature, and thus, the thermal efficiency.

The purpose of this study was to investigate and evaluate the effect that hexcan design changes have on the intra-assembly coolant flow and temperature distribution using state-of-the-art computational fluid dynamics (CFD)

simulation software to quantify the effect that the design changes have on heat transfer and fluid flow within the assembly subchannels. This approach has been used previously to investigate the pressure drop across a fast reactor subassembly and to evaluate various modeling options, including turbulence models.[8]

II. MODELING AND SIMULATION

Simulations were performed for a 19-pin fast reactor subassembly with wire wrap spacers. This is representative of experimental test subassemblies that have been used in the past.[9] Figure 1 shows a solid model of the fuel pins for this basic geometry, showing the spiral wire wrap on each pin. These fuel pins were placed inside a hexcan for the flow and temperature simulations. Several hexcan designs, with differences in the interior surface of the hexcan, were evaluated. High performance computers (HPCs) and commercial computer-aided engineering (CAE) tools, including computer-aided design (CAD) and computational fluid dynamic (CFD) software, were used during the modeling and simulation (M&S) process. Noteworthy is that advances in computational hardware and software over the last decade have provided engineers with advanced M&S tools making it now possible to simulate three dimensional complex geometries, such as fast reactor fuel pins with spiral wire wrap, using millions of computational elements on high performance computers.

A basic description of the modeling and simulation process is provided below; refer to Ref. 8 for the details of the modeling and simulation process used for this study.

II.A. Geometry and Mesh Generation

The subassembly geometry modeled is based on typical fuel pin design dimensions, similar to those used for the preconceptual design of the Advanced Burner Test Reactor (ABTR). Using the ABTR design as a guide, a reference subassembly design was created to compare the effects that modifying the hexcan interior design had on the temperature and velocity fields.[5] Figure 2 shows a typical subassembly geometry and associated nomenclature, which is consistent with that presented by Todreas and Kazimi.[10] For comparison purposes, Table I presents the nominal dimensions of the reference design and the ABTR subassembly design. Note that in this report and in the literature "spacer wire" and "wire wrap" are used interchangeably; additionally, "hexcan", "wrapper", and "flow duct" also are used interchangeably.

The wire wrap, used to promote coolant mixing and provide a means to separate fuel pins, is a wire of circular cross-section. For modeling and simulation purposes, due to the traditional difficulties of successfully calculating flows in small flow areas of narrow wall angle (as occurs when two cylinders are tangent to one another), different

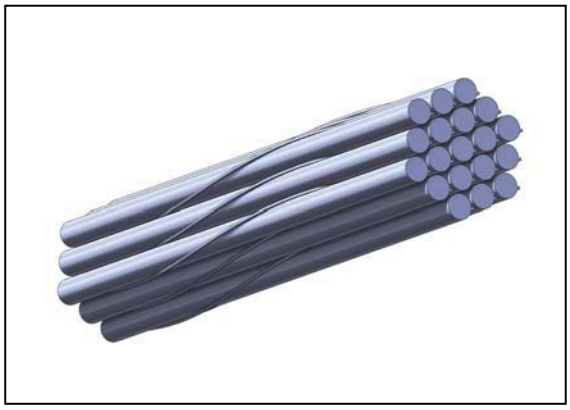

Fig. 1. 19-Pin Fast Reactor Subassembly Solid Model

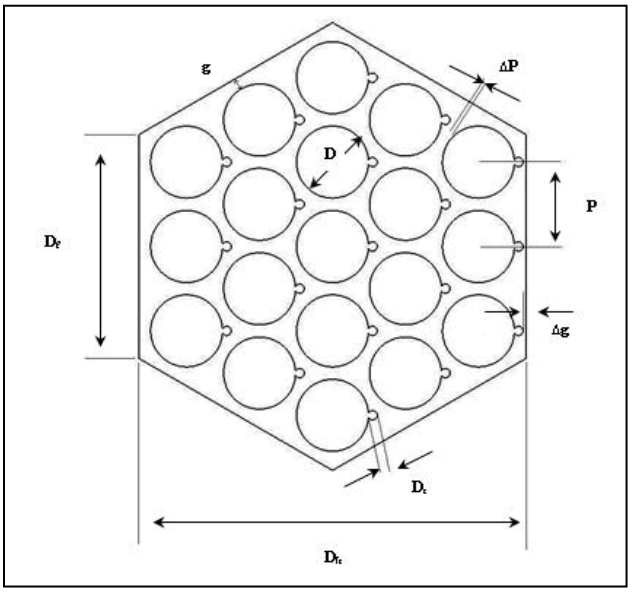

Fig. 2. 19-Pin Fast Reactor Geometry Description

cross-sections of the wire wrap were investigated to evaluate which would provide the best representation of the flow and temperature fields while resulting in the best numerical convergence for the simulations. The geometry chosen, shown in Fig. 3, was selected, to eliminate the very small flow areas with narrow wall angle, and to minimize the number of computational mesh elements (i.e. computational time) while still providing a realistic representation of the geometry. The CAD geometry and computational fluid volume (i.e. reference design), shown in Fig. 4, was created using SolidWorks, commercial software, and imported into STAR-CCM+, commercial CFD software, which was used to create the computational mesh and simulate the heat transfer and fluid-flow through the assembly.[11, 12]

Table I
Subassembly Nominal Dimensions

Model	ABTR	Reference Design
Pins	217	19
D	0.8	0.8
Ds	0.103	0.103
P/D	1.13	1.13
P	0.904	0.902
ΔP	0.001	0.005
Δg	0.033	0.005
D_{ft}	13.598	4.126
D_{f}	-	2.382
Length	260	20.32

Notes:
1. All dimensions in centimeters.
2. Geometry includes a pin-to-wire wrap overlap of 0.0065 cm

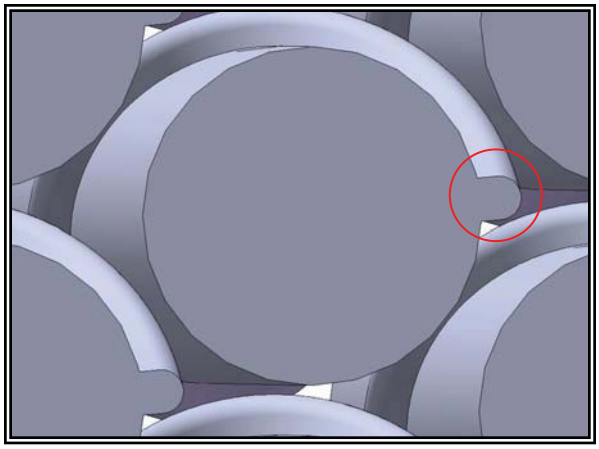

Fig. 3. Wire Wrap Profile Approximating Wire Wrap of Cylindrical Cross-Section

High performance computers were required to generate the hybrid meshes needed to predict secondary flows created by the helical wire wrap spacers; computational meshes ranging from 49 to 55 million elements were common for a single pitch of the wire wrap (i.e. the length of wire wrap required to complete a single revolution around the fuel pin). Computational requirements for meshing the geometry were significant. Contributing to this was the multi-length scale geometry and the desire to predict the complex fluid flow created by the wire wraps. The computational mesh was generated on a SGI Altix 4700 shared memory machine with 256 GB of memory and Intel Itanium 2 processors with a 1.5 GHz clock speed. Approximately 30 hours were required to generate each computational mesh.

II.B. Simulation Solver and Models

The following STAR-CCM+ simulation settings and models were used for the vertically oriented fuel assembly: 3-D, incompressible flow, "Realizable k-ε Two-Layer" turbulence model with "all y+ wall treatment," steady-state segregated solver, using a second order upwind convection scheme. Since the flow is incompressible (with the gravity model "enabled"), coupling between the momentum equation and energy equation is established using the Boussinesq approximation. Material properties for sodium at 700K, which is near the average coolant temperature of the ABTR were used.[13] Although the assumption of constant properties contributes to simulation uncertainty, its impact on the results is a topic for future studies.

The segregated solver was chosen due to previous experience using this solver for incompressible heat transfer and fluid flow simulations. Since this study was preliminary in nature and based on lessons-learned from the Ref. 8 study, the k-ε turbulence model was chosen knowing that reliable physical models for turbulent heat transfer for low Prandtl number fluids in complex geometries have yet to be validated. For example, Ref. 8 reported numerical noise while using the k-ω SST (Mentor) turbulence model; this noise was suppressed when the k-ε turbulence model used. Additionally, Ref. 14 discusses assessment of physical models for turbulent heat transfer to liquid metals. Nevertheless, evaluating the impact of turbulence models on simulation uncertainty was not the goal of this study. The "all y+ wall treatment" was chosen based on the recommended guidance provided in Ref. 12.

A uniform velocity of 2 m/s was specified at the fuel assembly inlet. The inlet velocity was increased in each design in order to maintain a constant mass flow rate of 0.92 kg/s, while maintaining turbulent flow within the computational domain; inlet temperature was specified at 680 K.[15] Turbulence parameters were estimated using guidance from Ref. 16. Inlet values of 0.05 for turbulence intensity and 0.3 mm for turbulent length scale were assigned; outlet turbulence parameters of 0.07 for turbulence intensity and 0.3 mm for turbulent length scale were assigned for the outlet conditions. A pressure of 0 psi was specified at the outlet. A constant heat flux of approximately 1.08 MW/m^2 was applied at the fuel pin boundaries; adiabatic conditions were specified at the wire wrap boundaries and the wrapper wall.

The HPC used to run the simulations was a SGI Altix ICE 8200 distributed memory machine with 2048 compute cores, 8 cores/node, 16 GB/node, and containing quad-core

Intel Xeon "Clovertown" processors with a 2.66 GHz clock speed. Simulation time was approximately 10 days using 128 processors.

Similar to Ref. 8, a general validation methodology was observed, although portions (beyond that used to guide development and use of the model) of the validation process such as spatial convergence studies and comparison with experimental data were not performed.[17] In short, the focus of this study was on trends in hydrodynamic parameters, including their effect on hot channel factors, which were evaluated in order to suggest an improved wrapper geometry. Predictions for velocity, temperature, and temperature distributions are shown.

III. HEXCAN DESIGNS

Five hexcan designs were evaluated for this study. All design changes were made with the fundamental goal of flattening the subassembly radial temperature profile in an effort to reduce peak-to-average radial temperature. This design process consisted of modifying the original design (Fig. 4) to restrict flow in the edge and corner subchannels.

The basic approach for modifying the wrapper design was to create additional flow restriction along the wrapper wall. Specifically, a third ring of "dummy" fuel elements intersected the two-ring subassembly. The solid-part overlap (i.e. blue protrusion), shown in Fig. 5, at the interface between the third ring and subassembly wrapper resulted in additional flow restriction. In short, additional flow restrictors were modeled on the subassembly wrapper to decrease the flow in the peripheral subchannels.

Design #1, the reference design, is shown in Fig. 4. The design is based on a subassembly with similar dimensions to that of the Advanced Burner Test Reactor (ABTR). Design #2 through Design #5 are similar in design to the base design, and differ only in the wrapper geometric profile (Fig. 6 through Fig. 8). Design #3 is not discussed in this report since it is similar to Design #5 but with larger edge and corner subchannel flow area.

Table I presents the geometric details of Design #1, including the ABTR geometry; a description of the geometry is shown in Fig. 1. Note that due to the complexity of obtaining a good quality mesh, simulations were not performed for Design #2. Specifically, the wire wrap protrusions, shown circled in Fig. 6, resulted in too complex of a meshing problem to pursue.

IV. SIMULATION RESULTS

The results, presented in two parts, include analyses for Design #1, Design #4 and Design #5. Part I of the study compares contour plots showing the effect that flow distribution has on outlet temperature. Part II of the study compares the radial temperature profiles of all designs analyzed. Additionally data related to nominal and peak temperatures are presented in tabular form along with the corresponding coolant hot channel factors.

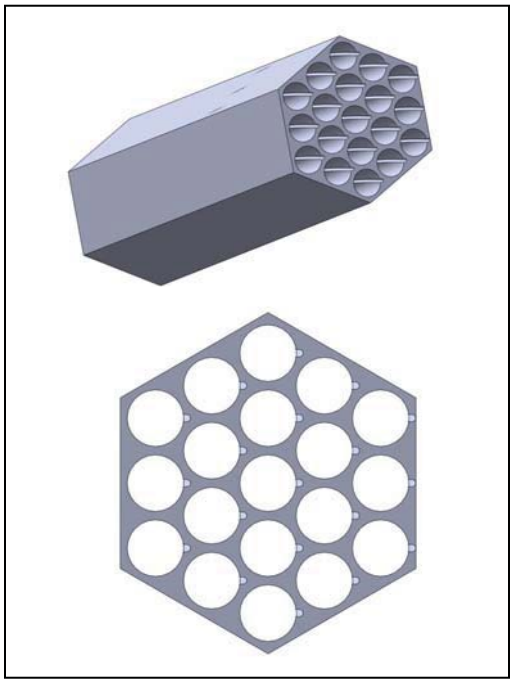

Fig. 4: Computational Fluid Volume (Design #1)

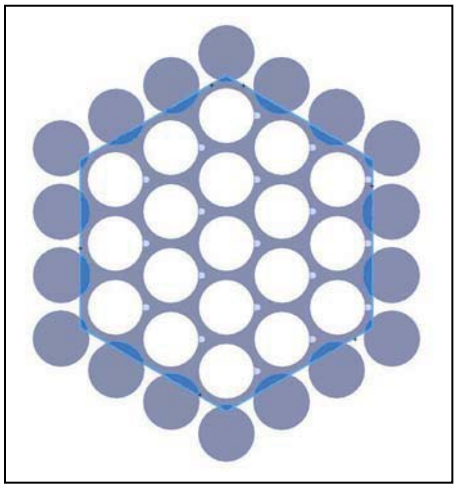

Fig. 5. Flow Restrictor Model

Although numerous variables are available for post-processing of results, four primary analysis metrics were used to evaluate the results: outlet velocity magnitude contours, outlet temperature contours, peak-to-average temperature plots, and coolant temperature rise hot channel factors. Figure 9 shows the line probes used to extract temperature data on the subassembly outlet face of each

design; using the probe, numerous data points were extracted. Similar to the temperature distribution analyses in Ref. 3, two temperature distributions were analyzed: a flat-to-flat profile along "dashed red line" and a diagonal profile along the "solid red line".

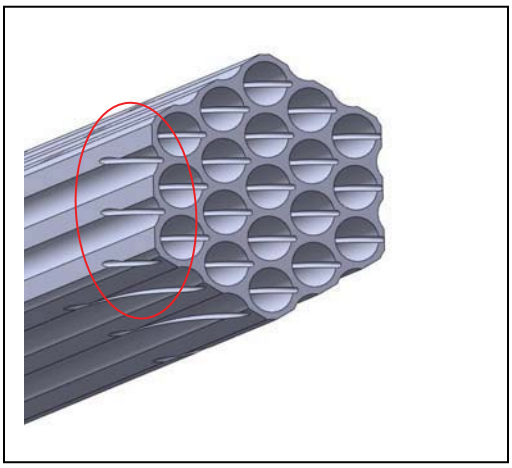

Fig. 6. Computational Fluid Volume (Design #2)

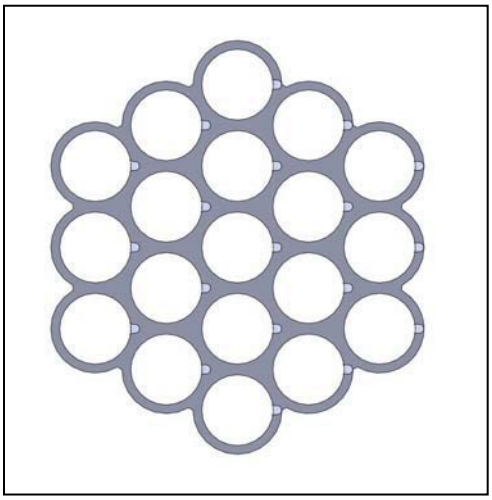

Fig. 7. Computational Fluid Volume (Design #4)

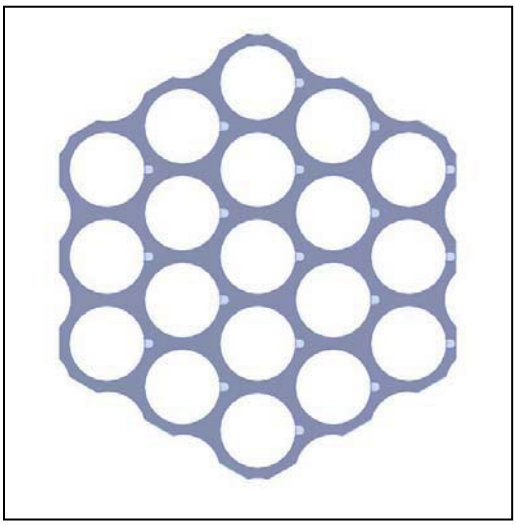

Fig. 8. Computational Fluid Volume (Design #5)

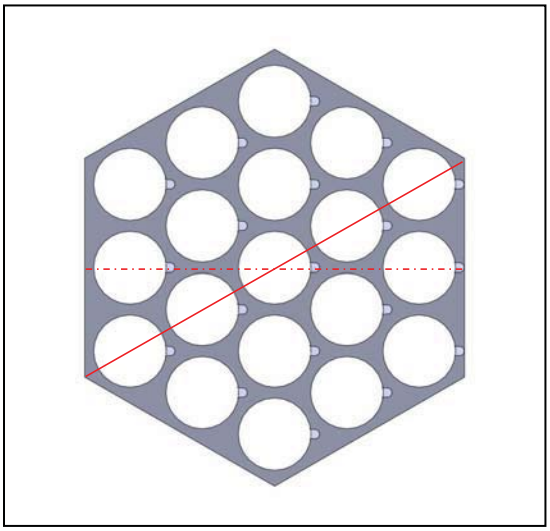

Fig. 9. Line Probes

V. SIMULATION OBSERVATIONS

Part I results are presented in Fig. 10 and Fig. 11. Figure 10 is a contour plot of velocity magnitude for each hexcan design. In order to depict the effect that design changes have on flow area, contour ranges were post-processed using the same maximum and minimum velocity predicted by Design #1. Note the large velocities in the outer subchannels of Design #1 and how by simply reducing the peripheral flow area, results in a larger percentage of the total flow being directed to the inner subchannels of Design #5 and Design #4.

The impact on temperature distribution, as the result of the design changes, is shown in Fig. 11. For comparison purposes and in order to better depict the effect that the design changes have on establishing a more uniform temperature distribution, the results were post-processed with the same maximum and minimum temperatures predicted by Design #1. Note the effect on the temperature distribution as the outer subchannel flow area is incrementally reduced in each design. Specifically, as you transition from Design #1 to Design #4, the coolant flow area next to the hexcan wall decreases as compared to flow

area in the interior of the subassembly. This results in a lower flow rate near the hexcan wall, more cooling in the interior subchannels, resulting in a more uniform temperature distribution.

Part II of the study approaches the research from a more "quantitative" perspective. The results are presented in Fig. 12 through Fig. 16, Table II and Table III. Figure 12 and Figure 13 are graphs of peak-to-average temperature profiles obtained from temperature data extracted from the flat-to-flat and diagonal line probes. Design #1 is shown in red diamonds, Design #5 in blue asterisks, and Design #4 in green triangles. As expected, the flow area reduction in the edge and corner subchannels (i.e. outer subchannels) results in the reduction of the peak-to-average temperature in the inner subchannels while the peak-to-average temperature increases in the outer subchannels, providing a more uniform temperature distribution. The sinusoidal behavior of peak-to-average temperature is the result of higher flow in interior subchannels and lower flow at the interface between interior subchannels; the Design #1 velocity magnitude contour plot in Fig. 10 depicts this phenomena. Table II presents the average and peak temperature results. Consistency between simulations is shown as average ΔT remains approximately the same for each design; furthermore, the peak temperature data indicates that the design changes result in lower peak temperatures for a given inlet temperature. The reason for the one degree average outlet temperature difference for Design #5 is not known; additional checks were performed in an effort to determine the cause, including analyzing mesh metrics, boundary conditions and reverse flow conditions.

Additional temperature results are presented in Fig. 14 through Fig. 16 and Table III. Figure 14 is a graph of peak-to-average temperature profiles obtained from temperature data extracted from the line probes for Design #1. Trendlines, obtained using n^{th} order polynomial approximations, are shown as black dashed lines; average coolant temperature is plotted as a horizontal green line. Note that the trends of these plots are similar to those presented in Figure 10-9 of Ref. 3. Similar to Fig. 12 and Fig. 13, the peak temperature is larger in the inner subchannels while the peak temperature is lower edge subchannel. Figure 16 shows the "optimal" effect of the design change of reducing outer subchannel flow area. Specifically, peak temperatures are reduced in the inner subchannels while peak temperature is increased in corner subchannels, resulting in a more uniform temperature profile compared to other designs.

The methodology used to compute hot channel factors (HCFs) in this study is similar to that used to describe the application of (HCFs) in Ref. 3. Table III presents the peak temperature data used to compute HCFs; average values required for the calculations were obtained from Table II. The total coolant temperature rise hot channel factor, F_b, and the assembly maldistribution factor (AMF), which represents the contribution of the differences between interior and edge flow channels within an assembly to the total HCF, were computed. The variables used to compute the HCFs are presented in Equations 1-3.

$$\Delta T_{max} = (\Delta T_{avg})(F_b)(PF) \quad (1)$$

$$F_b = (F_d)(F_s) \qquad \text{where } F_s = 1.08 \quad (2)$$

$$F_d = (AMF)(1.03)(1.05) \quad (3)$$

The first step in the process was to compute an overpower factor (PF) using F_b=1.26 and data presented in Table II and Table III, for Design #1. The purpose of this step was to "match" the reference design (i.e. Design #1) HCF parameters to those presented in Ref. 3 for the Clinch River Breeder Reactor Project (CRBRP); specifically, the goal was to ensure that F_b=1.26 and that AMF=1.08 for the reference design. An overpower factor of 1.13 resulted in "matching" hot channel factors for Design #1 and the CRBRP.

Using the same process described above, F_b and AMF were computed for Design #4 and Design #5. The calculations resulted in AMF values less than one, so the AMF values for these designs were set to a value of 1.00. In order to estimate the temperature rise that could be possible as a result of the wrapper design changes, the overpower factor was increased from 1.13 to 1.15, which is the design value specified in Ref. 3.

The calculations showed that the total HCF for Design #4 and Design #5 decreased by approximately 7%, indicating that a temperature rise of approximately 14 ^{o}C and a corresponding increase in thermal efficiency of 1% may be possible. The results are presented in Table III.

VI. CONCLUSIONS

The results of this study show that by modifying the standard hexcan design, the radial temperature distribution of a fast reactor fuel assembly can be flattened, reducing thermal stresses and the peak-to-average temperature. This reduction in the outer perimeter flow area indicates that it may be possible to raise the average coolant outlet temperature by approximately 14 ^{o}C without increasing the peak temperatures within the subassembly, ultimately resulting in improved thermal efficiency for fast reactor designs.

Future studies are planned to improve the 19-pin assembly model by adding fuel, sodium bond, and cladding for each fuel element in order to reduce simulation uncertainties in subassembly temperature distributions. For example, it is expected that the thermal streaking between adjacent fuel pins and wire wraps, observed in Fig. 12 of Ref. 8, would be eliminated because a conjugate heat transfer analysis would accurately predict circumferential heat transfer within the solid cladding.

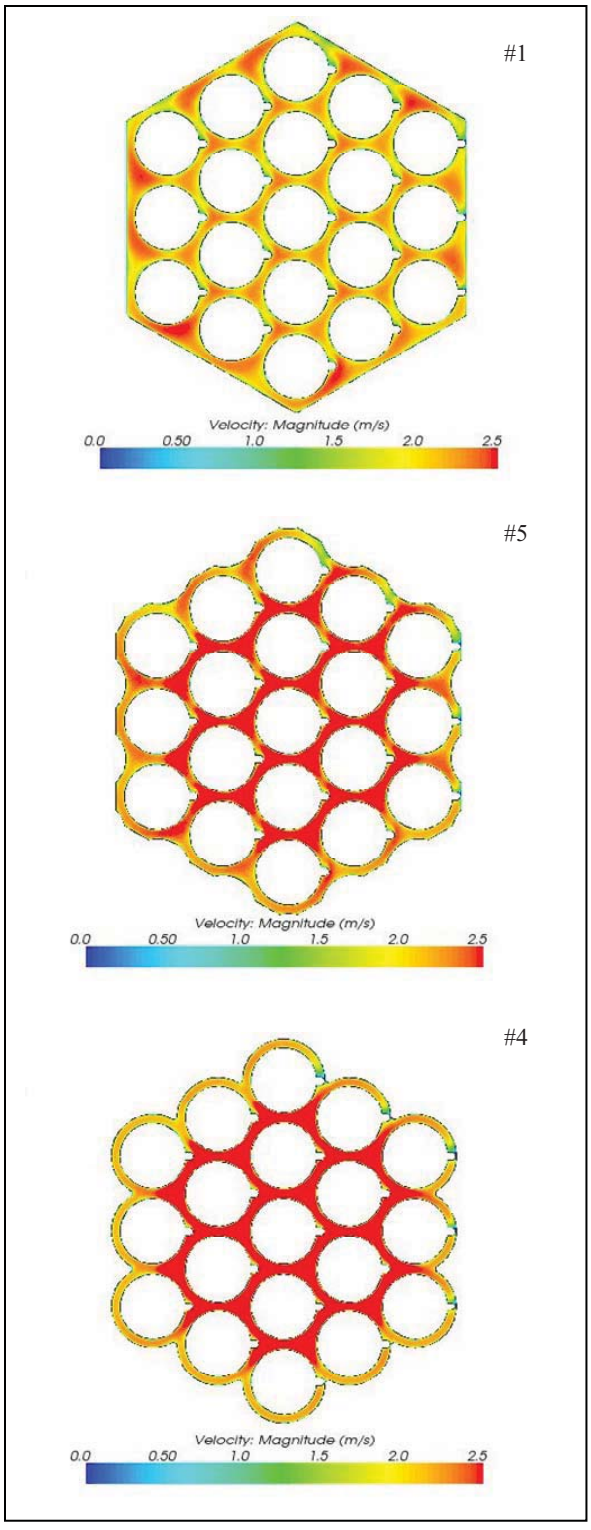

Fig. 10. Velocity Contours (Designs #1, #5, #4)

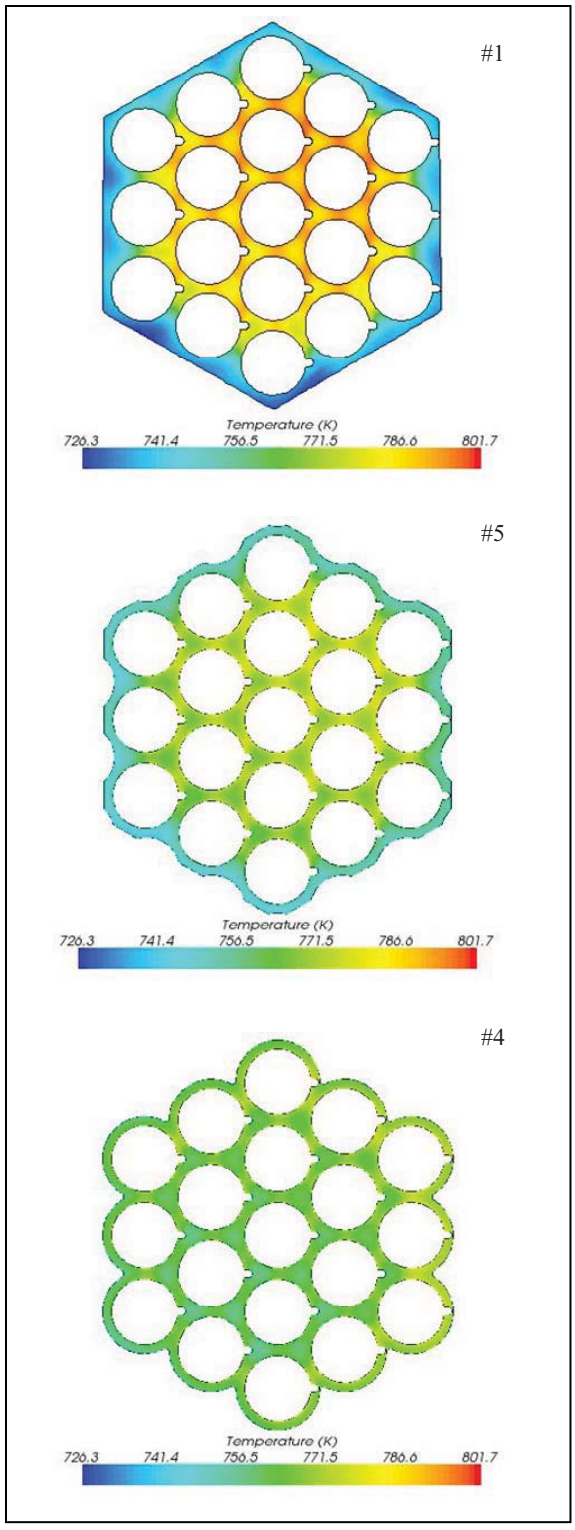

Fig. 11. Temperature Contours (Designs #1, #5, #4)

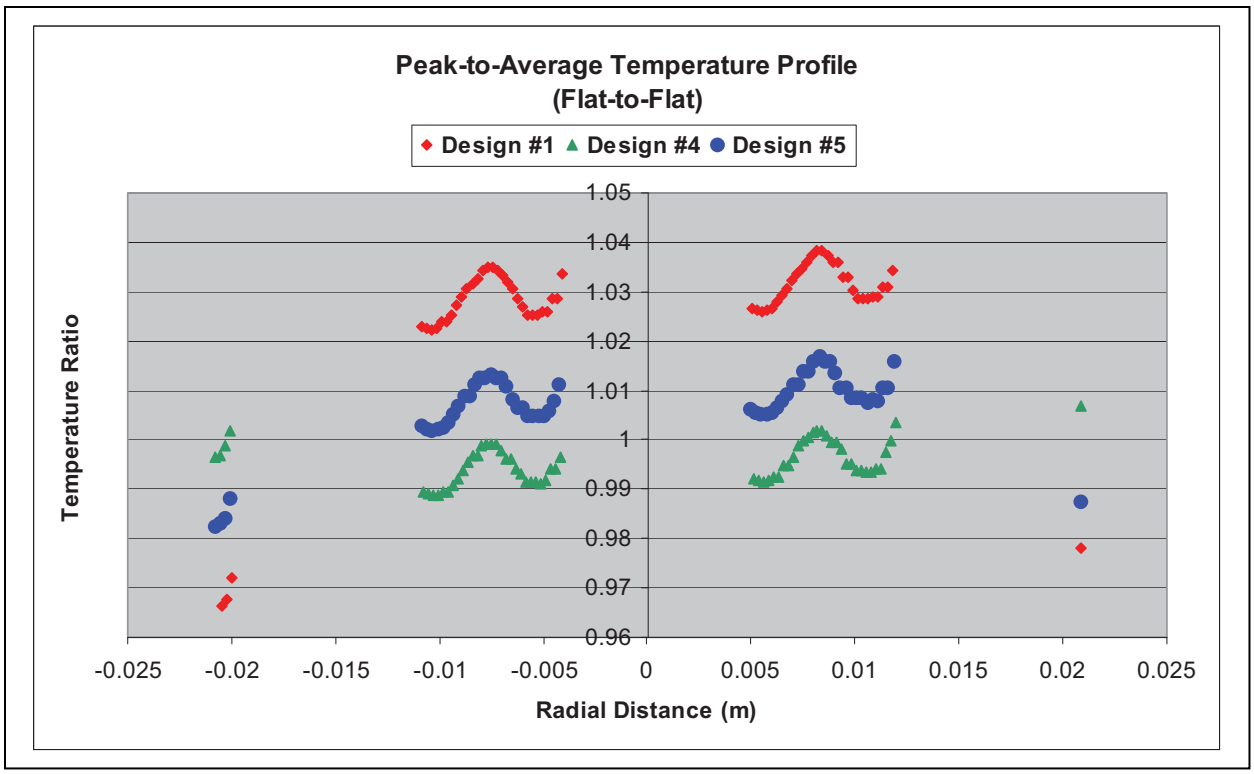

Fig. 12. Peak-to-Average Temperature (#1, #4, #5)

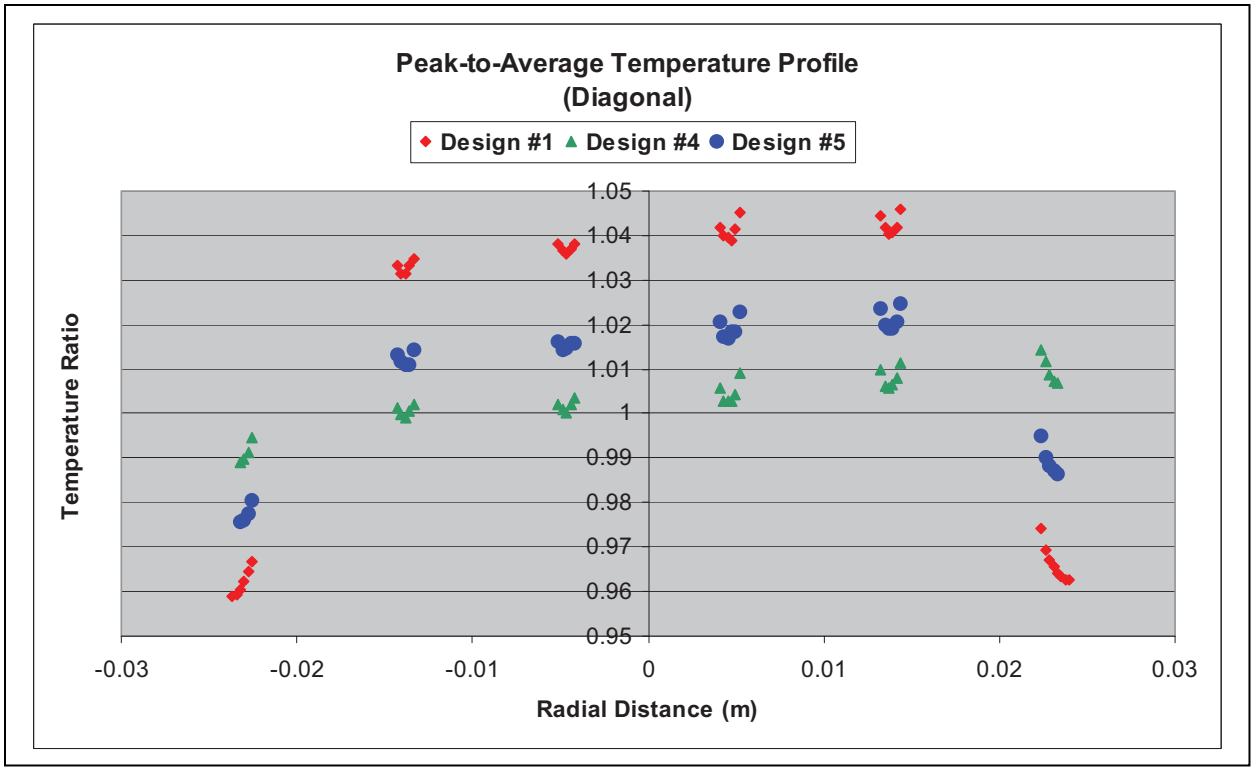

Fig. 13. Peak-to-Average Temperature (#1, #4, #5)

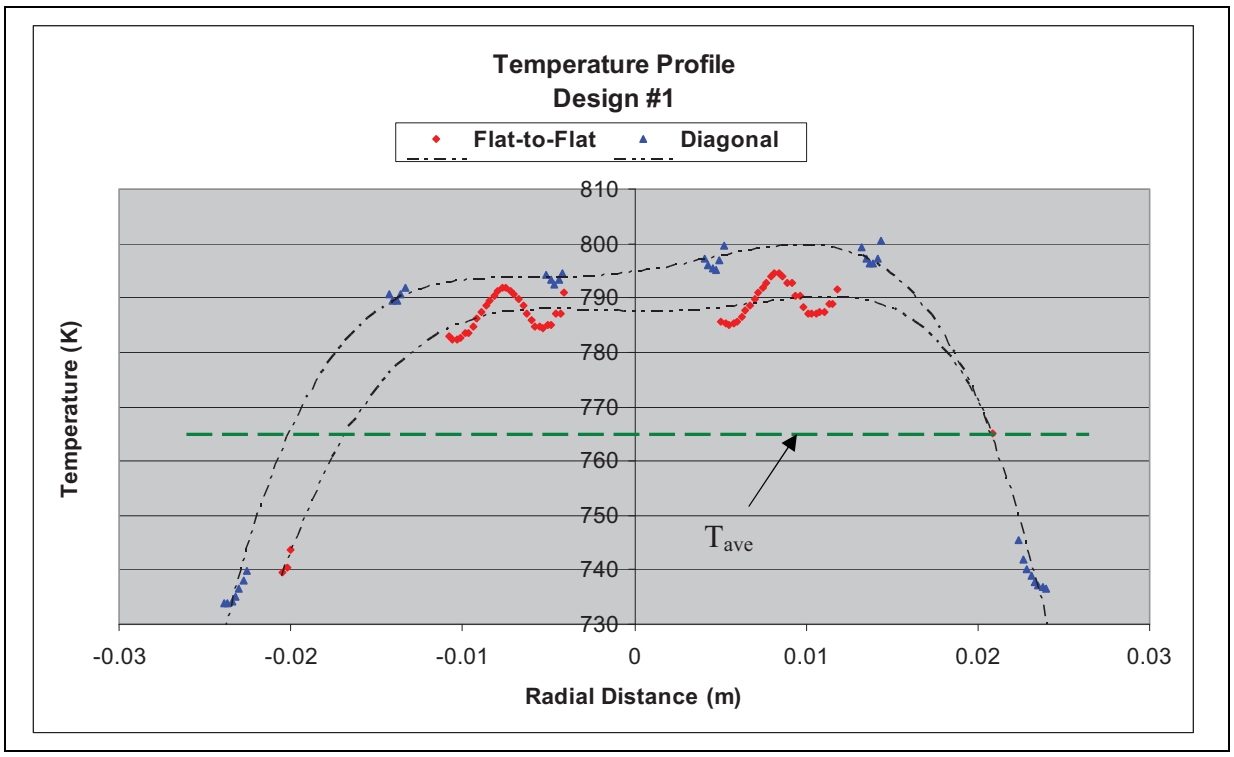

Fig. 14. Design #1 Temperatures

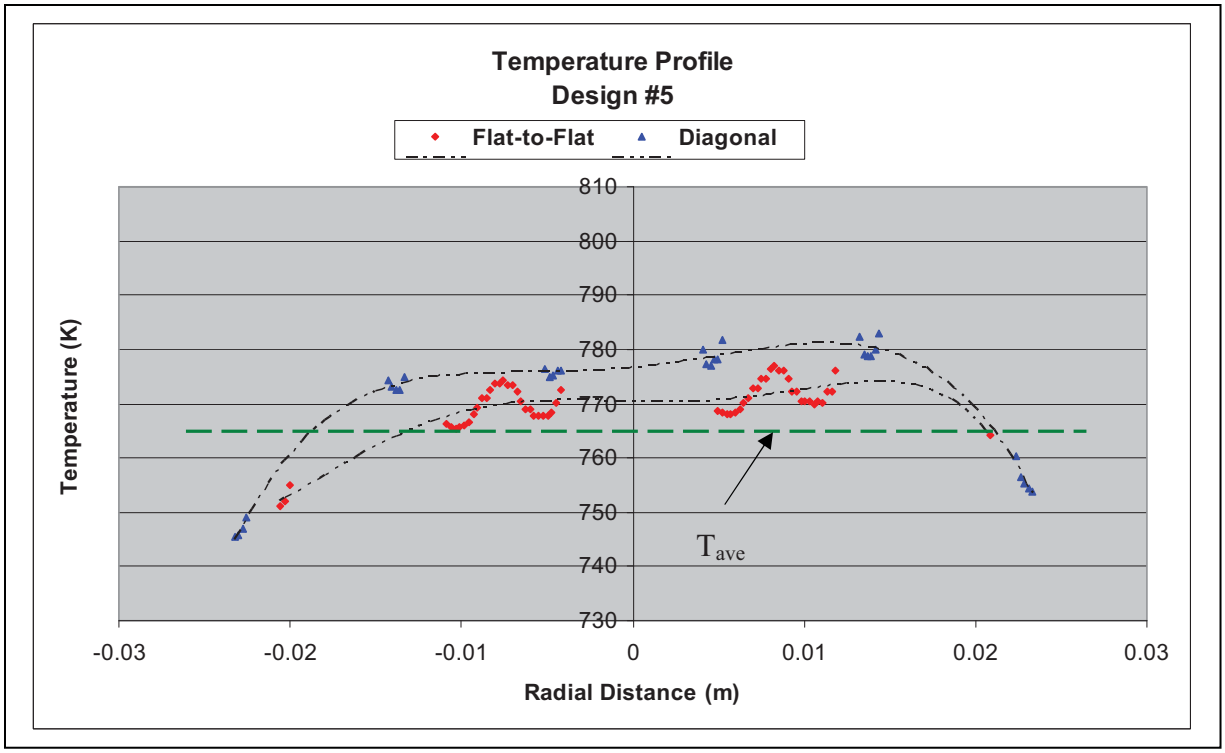

Fig. 15. Design #5 Temperatures

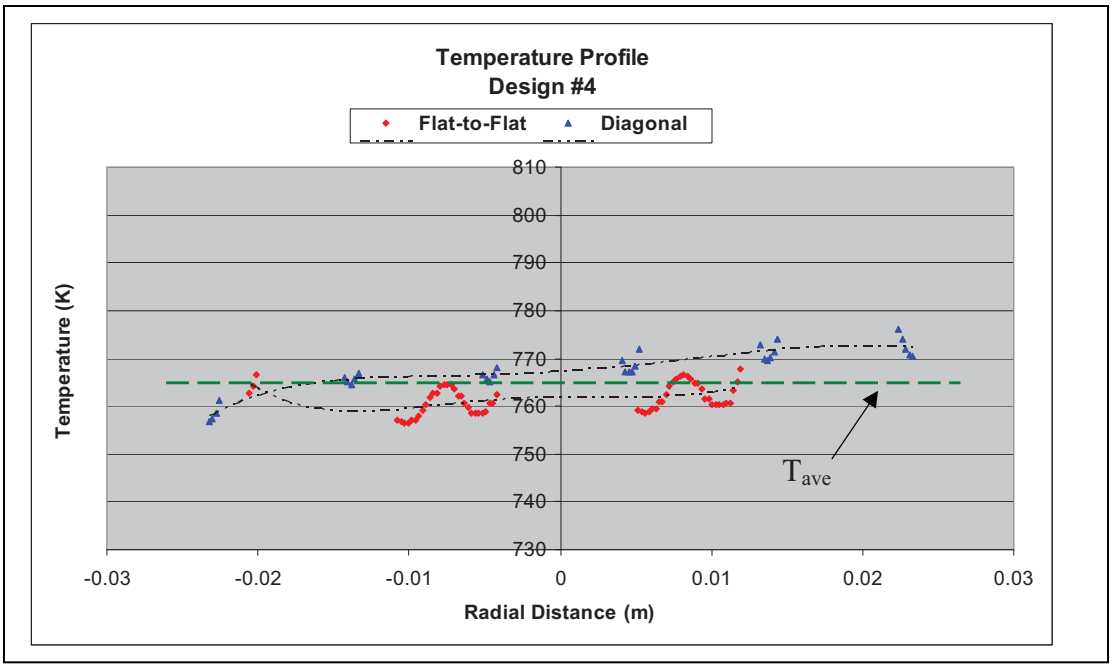

Fig. 16. Design #4 Temperatures

Table II
Temperature Data

	Average Temperature (K)			Peak Temperature (K)		
Design	Inlet	Outlet	ΔT	Inlet	Outlet	ΔT
#1	680.0	765.2	85.2	680.0	801.7	121.7
#4	680.0	765.1	85.1	680.0	779.9	99.9
#5	680.0	764.1	84.1	680.0	784.0	104.0

Table III
Hot Channel Factor Data

	Peak Temp. (K)	Hot Channel Factor (PF = 1.13)			Temp. Increase (PF = 1.15)
Design	Outlet	F_b	AFM	%Δ	ΔT
#1	801.7	1.26	1.08	N/A	N/A
#4	779.9	1.17	1.00	-7.1	14.6
#5	784.0	1.17	1.00	-7.1	9.2

NOMENCLATURE

D	pin nominal diameter
D_s	wire-wrap nominal diameter
D_ℓ	assembly flat nominal length
D_{ft}	assembly flat-to-flat nominal distance
P	pin pitch
ΔP	clearance per interior pin
g	outer ring pin-to-wrapper clearance
Δg	outer ring wire-wrap to wrapper clearance
K	Kelvin
F_b	coolant temperature rise hot channel factor
F_d	direct combination factor
F_s	statistical combination factor
ΔT	differential temperature
PF	overpower factor
AMF	assembly flow maldistribution factor
%Δ	percent change
°C	degrees Celsius

REFERENCES

1. Y. K. PETRENYA, L. A. Khomenok, P. A. Kruglikov and Y. V. Smolkin, "Lines of improving the economic efficiency of nuclear power stations equipped with VVER Reactors," *Thermal Engineering*, **Vol. 54**, *No. 1*, 32-35, (2007).

2. M. ICHIMIYA, T. Mizuno and S. Kotake, "A Next Generation Sodium-Cooled Fast Reactor Concept and Its R&D Program," *Korean Nuclear Society*, **Vol. 39**, *No. 3*, 171-186, (2007).

3. A. E. WALTAR and A. B. Reynolds, *Fast Breeder Reactors*, Chapter 10, Pergamon Press, New York, (1981).

4. J. YOO, Y. Oka, Y. Ishiwatari, J. Yang, and J. Liu, "Subchannel analysis of supercritical light water-cooled fast reactor assembly*," Nuclear Engineering and Design*, **Vol. 237**, *No. 10*, 1096-1105 (2006).

5. Y. I. CHANG, P. J. Finck, and C. Grandy, *Advanced Burner Test Reactor Preconceptual Design Report,* ANL-ABR-1, Argonne National Laboratory, (2006).

6. A. OTSUBO, T. Okada, N. Takahashi, K. Soto and N. Hattori., "The Occurrence of Wear Marks on Fast Reactor Fuel Pin Cladding," *Journal of Nuclear Science and Technology*, **Vol. 36**, *No. 6*, 522, (1999).

7. M. W. ASHTON, "*Nuclear Reactor Fuel element Sub-Assemblies*," Patent Specification, No. 1419073, London Patent Office, (1973).

8. K. D. HAMMAN and R. A. Berry, "A CFD Simulation Process for Fast Reactor Assemblies", *Proceedings of Experiments and CFD Code Applications to Nuclear Reactor Safety (XCFD4NRS 2008)*, Grenoble, France (2008).

9. E. H. NOVENDSTERN, "Turbulent Flow Pressure Drop Model for Fuel Ford Assemblies Utilizing a Helical Wire-Wrap Spacer System," *Nuclear Engineering and Design*, Vol. 22, 19, (1972)

10. N. E. TODREAS and M. S. Kazimi, *Nuclear Systems II, Elements of Thermal Hydraulic Design*, Taylor and Francis, pp. 164-166, Boca Raton, Florida, (2001).

11. SolidWorks 2008, SolidWorks Corporation, www.solidworks.com .

12. CD-adapco, STAR-CCM+ User Guide, Version 3.06.006, CD-adapco, New York, 2008.

13. J. K. FINK and L. Leibowitz, *Thermodynamic and Transport Properties of Sodium Liquid and Vapor*, ANL/RE-95/2, Argonne National Laboratory, (1995).

14. X. CHENG and N. Tak, "Investigation on Heat Transfer to Lead-Bismuth Eutectic Flows in Circular Tubes for Nuclear Applications", *Nuclear Engineering and Design*, **Vol. 236**, *No. 4*, 385-393, (2006).

15. S. CHENG and N. E. Todreas, "Hydrodynamic Models And Correlations For Bare And Wire-Wrapped Hexagonal Rod Bundles-Bundle Friction Factors, Subchannel Friction Factors And Mixing Parameters", *Nuclear Engineering and Design*, **Vol. 92**, 227-251, (1986).

16. *CFD Online, "Estimating* Turbulence Intensity", www.cfd-online.com/Wiki/Turbulence_intensity, accessed February 2009.

17. AIAA, "Guide for the Verification and Validation of Computational Fluid Dynamics Simulations (AIAA G-077-1998)", Reston, New York (2002).